Supplementary Figures:
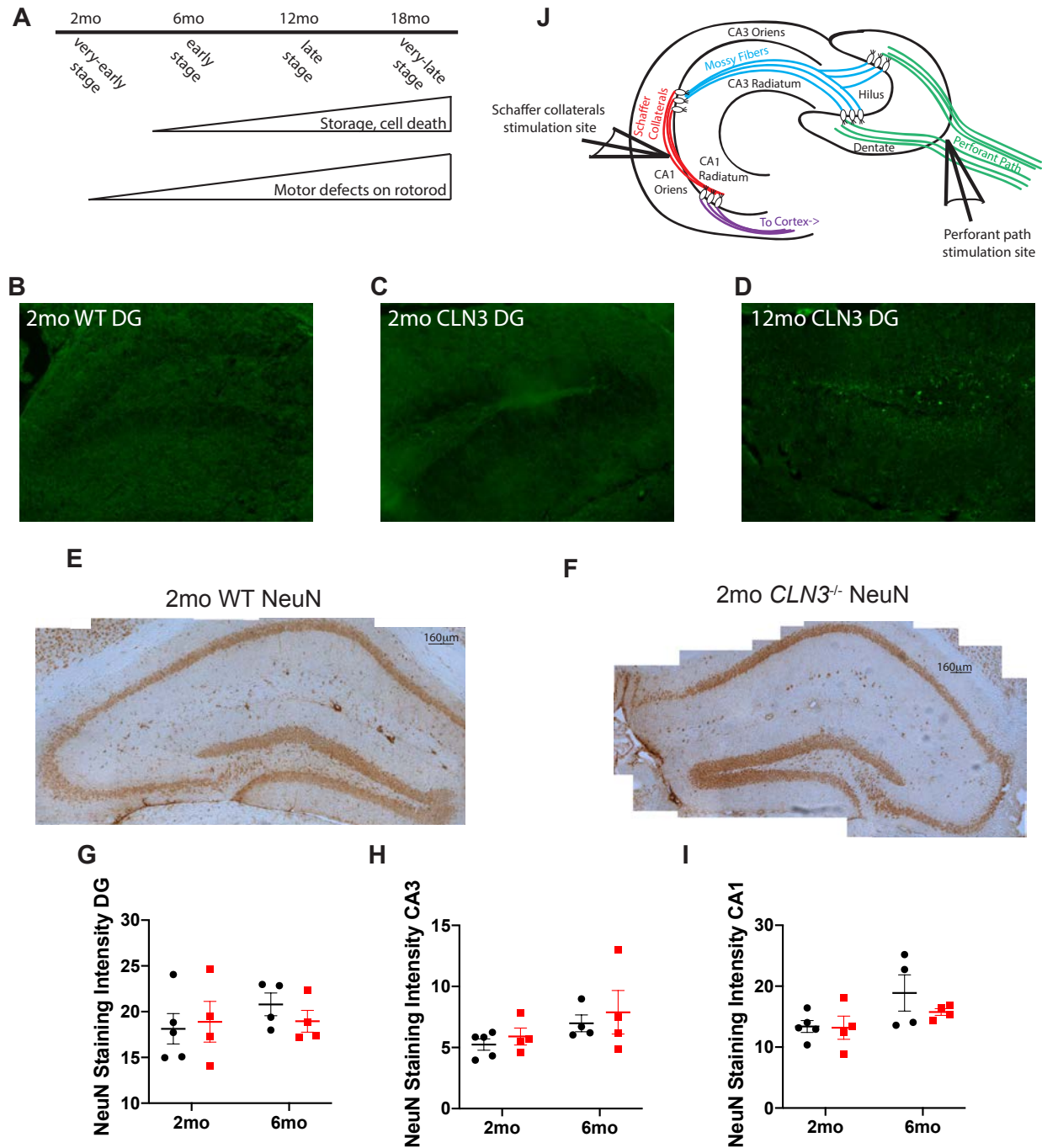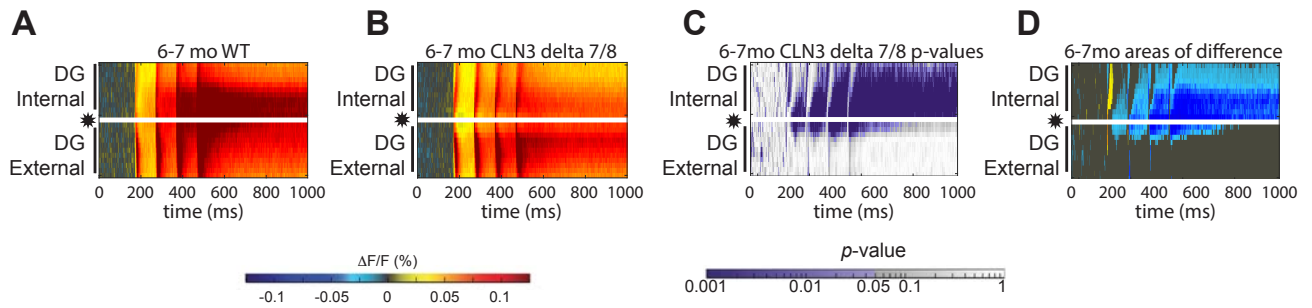

Supplementary Figure 1: In early-stage disease there is no storage accumulation or neuronal loss. (A) Timeline of disease progression in the *CLN3*$^{-/-}$ mouse. **(B-D)** Representative 10X images of the dentate gyrus (DG) show little autofluorescent storage material in 2-month-old WT or CLN3 disease mice. However, by 12 months, there is substantial accumulation. **(E-I)** At 2-months of age there is no CLN3-disease

associated difference in staining of the neuronal marker NeuN in any of the major hippocampal subfields. **E-F** are representative NeuN images. **G-I** are quantification of staining intensity. N=4-5 animals / condition, mean +/- SEM shown, two-way ANOVA all p-values >0.05. **(J)** Schematic of hippocampal circuit and location of electrode placement for perforant path (as in studies of Fig. 1,2,4,5) and Schaffer collateral (as in studies of Fig. 3) stimulation studies.

Dentate Gyrus after PP stimulation
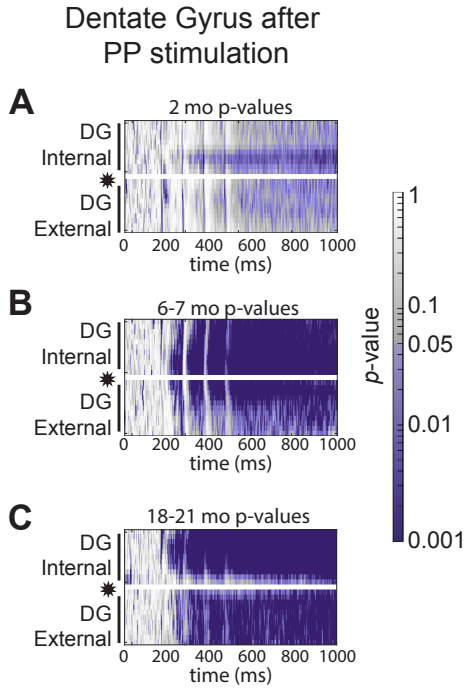
Supplementary Figure 2: *p*-value maps confirm decreased activation of the dentate gyrus in response to PP stimulation in *CLN3*$^{-/-}$ mice.
Results of permutation sampling statistical analysis (1000 permutations) of data from Figure 1 are shown with *p*-values <0.05 in purple. Dentate gyrus activation in response to perforant path stimulation is statistically different between WT and *CLN3*$^{-/-}$ slices at **(A)** 2 months, with more regions of statistical difference in the internal blade as compared to the external blade of the DG, **(B)** 6-7 months, and **(C)** 18-21 months of age. Group sizes (n=slices, N=mice): 2mo WT n=24, N=6; 2mo *CLN3*$^{-/-}$ n=26, N=5; 6-7mo WT n=23, N=5; 6-7mo *CLN3*$^{-/-}$ n=30, N=8; 18-21mo WT n=25, N=7; 18-21mo CLN3 n=26, N=7.

Supplementary Figure 3: The *CLN3*$^{\Delta ex7/8}$ mouse, which models the most common human CLN3 mutation, also demonstrates hypoexcitability of the dentate gyrus early in the disease course.
(A) Stimulation of the perforant path (location indicated by star) reveals robust excitation of the dentate gyrus (DG) in 6-7 month-old wild-type (WT) hippocampal slices, shown as a raster plot of average fluorescence change ($\Delta F/F_{WT}$). **(B)** By 6-7 months of age, the *CLN3*$^{\Delta ex7/8}$ DG is hypoexcitable (as measured by $\Delta F/F_{CLN3KO}$) as compared to WT after PP stimulation. **(C)** Results of permutation sampling statistical analysis (1000 permutations) comparing WT and *CLN3*$^{\Delta ex7/8}$ mice are shown with *p*-values <0.05 in purple. **(D)** . Regions of the raster plot with p>0.05 are masked in gray. For regions with p<0.05, the difference in fluorescence change ($\Delta F/F_{WT}-\Delta F/F_{CLN3KO}$) is shown. Cooler colors indicate relative hypoexcitability of the *CLN3*$^{\Delta ex7/8}$ DG. Group sizes (n=slices, N=mice): WT n=18, N=4; *CLN3*$^{-/-}$ n=24, N=5. Panel A reproduced from Figure 1D.

CA Stratum Radiatum after PP stimulation
CA Stratum Radiatum after SC stimulation
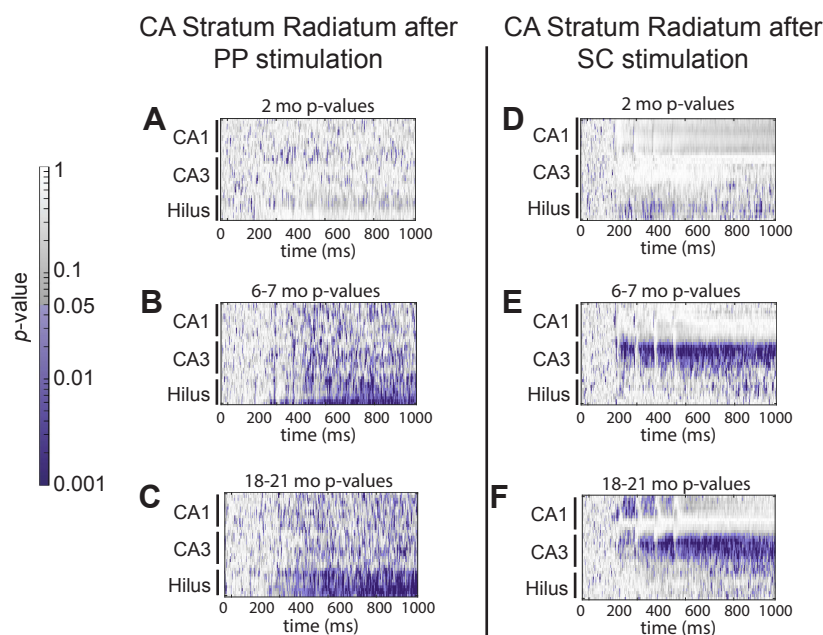
Supplementary Figure 4: *p*-value maps comparing activation of the CA stratum radiatum of WT and *CLN3*$^{-/-}$ mice in response to perforant path (PP) and Schaffer collateral (SC) stimulation.

Results of permutation sampling statistical analysis (1000 permutations) of data from Figure 2 and 3 are shown with *p*-values <0.05 in purple. Hilus, CA3 and CA1 activation in response to perforant path stimulation is minimally different between WT and *CLN3*$^{-/-}$ slices at **(A)** 2 months. However, statistically significant regions of hypoexcitability in *CLN3*$^{-/-}$ slices is apparent at **(B)** 6-7 months, and **(C)** 18-21 months of age. Group sizes panels A-C (n=slices, N=mice): 2mo WT n=24, N=6; 2mo *CLN3*$^{-/-}$ n=26, N=5; 6-7mo WT n=23, N=5; 6-7mo *CLN3*$^{-/-}$ n=30, N=8; 18-21mo WT n=25, N=7; 18-21mo CLN3 n=26, N=7. Similar results are seen in response to SC stimulation, with minimal differences at **(D)** 2 months, but clear genotype-associated differences at **(E)** 6-7 months, and **(F)** 18-21 months of age. Group sizes panels D-F (n=slices, N=mice): 2mo WT n=13, N=5; 2mo *CLN3*$^{-/-}$ n=11, N=5; 6-7mo WT n=13, N=4; 6-7mo *CLN3*$^{-/-}$ n=11, N=3; 18-21mo WT n=13, N=4; 18-21mo *CLN3*$^{-/-}$ n=14, N=4.
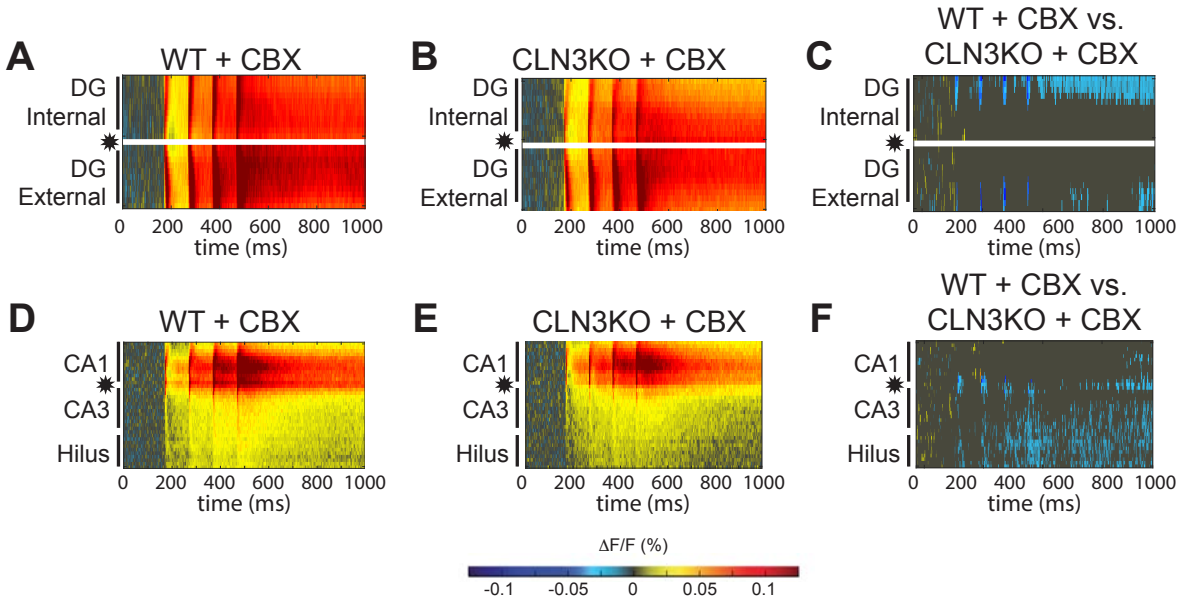
Supplementary Figure 5: Carbenoxolone (CBX), a drug that reduces storage burden, cannot correct hypoexcitability of the dentate gyrus, and worsens hypoexcitability of the hilus and CA3 in early-stage CLN3 disease.

(A-C) Hippocampal slices from 2-month-old mice treated with 2 weeks of 20mg CBX, a dose that reduces storage burden and normalizes endocytosis in vivo, show residual hypoexcitability of the dentate gyrus after perforant path (PP) stimulation, as measured by fluorescence response in CBX-treated WT vs $CLN3^{-/-}$ slices. **(D-F)** The hilus and CA3 regions of slices from CBX-treated $CLN3^{-/-}$ mice showed worsening hypoexcitability after Schaffer collateral (SC) stimulation. Group sizes (n=slices, N=mice): 2mo PP stimulation WT n=15, N=3; 2mo PP stimulation $CLN3^{-/-}$ n=25, N=5; 2mo SC stimulation WT n=17, N=4; 2mo SC stimulation $CLN3^{-/-}$ n=20, N=5. Areas of statistical significance identified using a permutation sampling method with 1000 permutations, for regions of significance with $p<0.05$, the difference in fluorescence change ($\Delta F/F_{WT}-\Delta F/F_{CLN3KO}$) is shown. Panel B reproduced from Figure 5B. Panel E reproduced from Figure 5E.
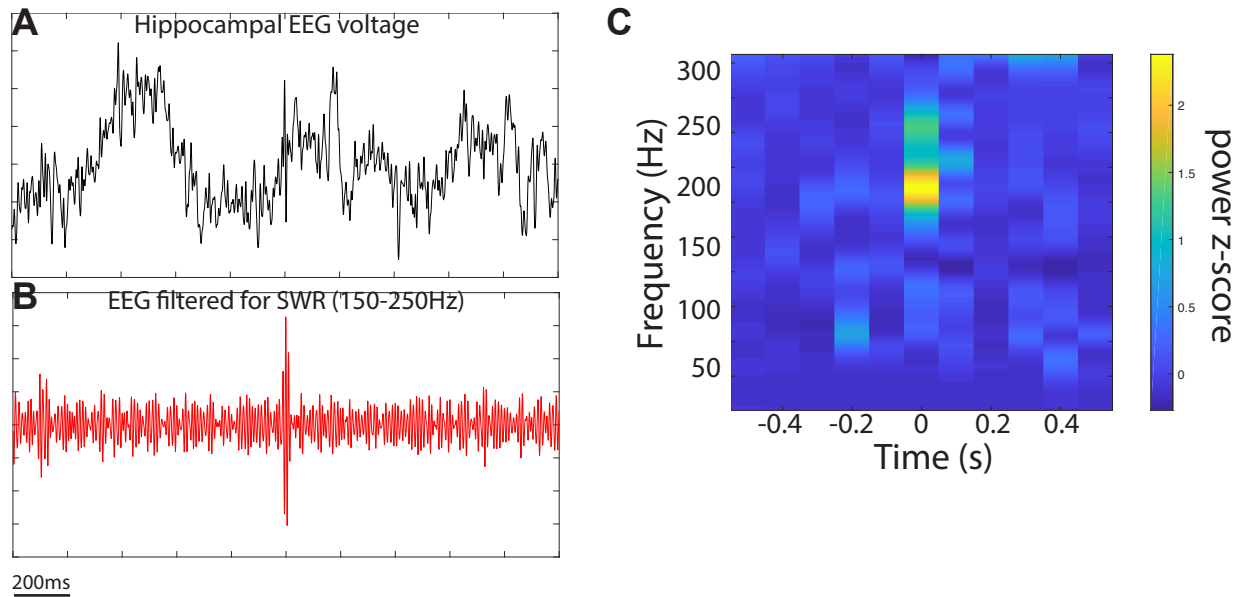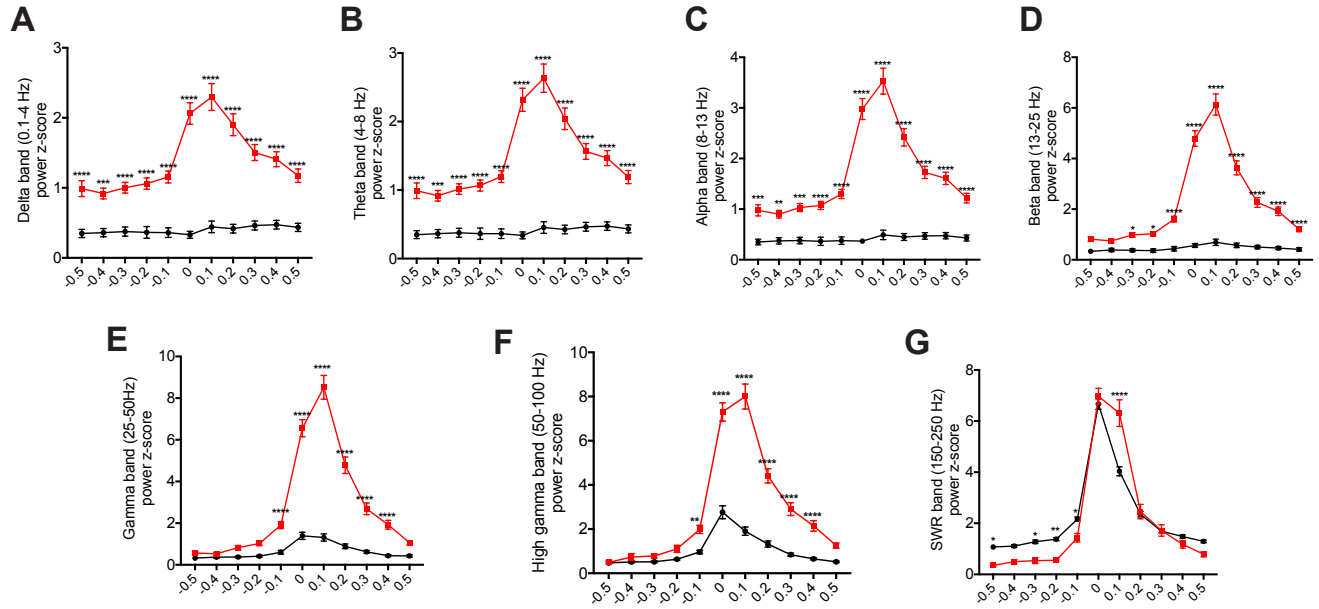
Supplementary Figure 6: Example sharp wave ripple (SWR) detection from a WT animal.

(**A**) Example 2 second raw EEG recording and (**B**) EEG signal filtered at 150-250Hz to show a SWR. (**C**) Example spectrogram analysis of the 1 second surrounding a SWR peak recorded from a WT hippocampus.
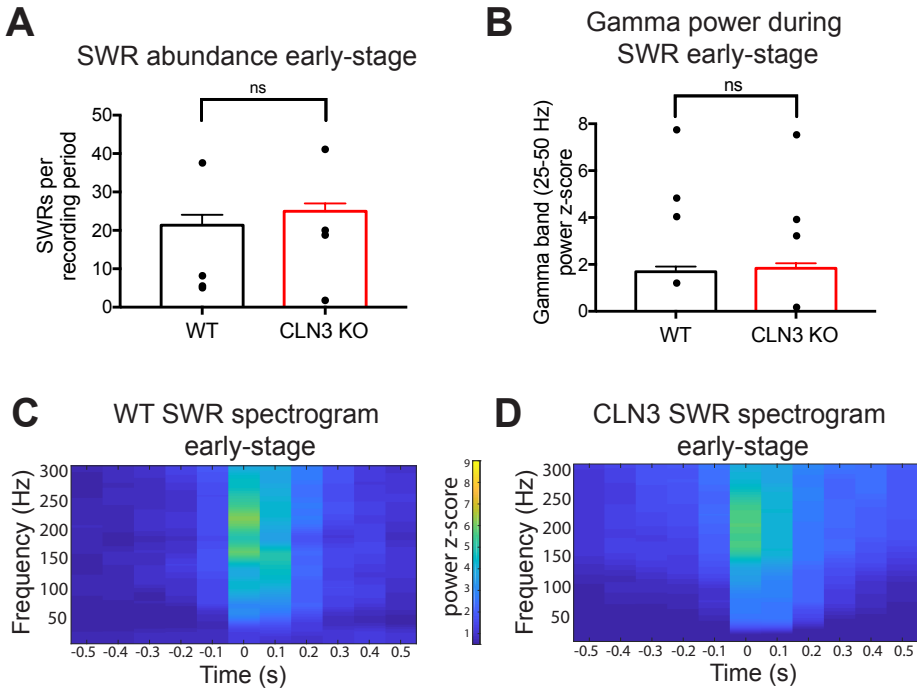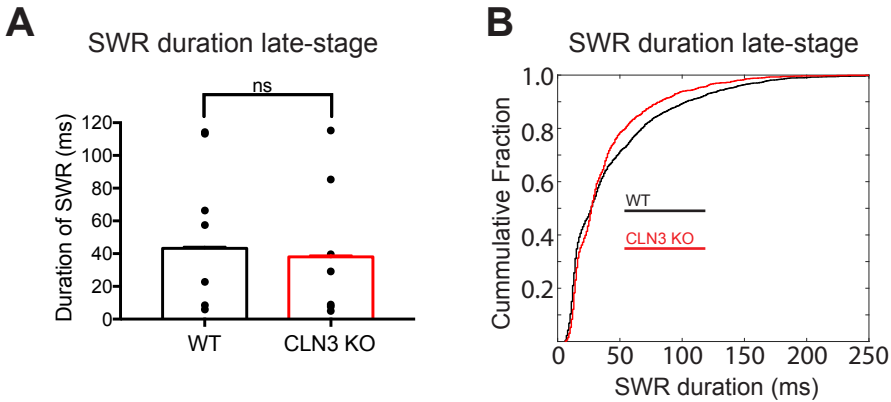
Supplementary Figure 7: In early stage disease there are no differences between WT and *CLN3⁻ᐟ⁻* hippocampal sharp wave ripple (SWR) abundance or gamma power modulation during SWRs.

(A) Quantification of SWRs per 30 min recording period from hippocampal EEG recordings of 6-month-old WT (black) and *CLN3⁻ᐟ⁻* (red) mice reveals no difference in SWR abundance (Mann-Whitney test *p*=0.51). (**B**) There was also difference in peak gamma power during an SWR (two-way ANOVA to evaluate animal and genotype variation, p=0.02 for genotype effect). **(C-D)** Average spectrograms from SWRs are similar between 6-month-old WT and CLN3 mice. Group sizes WT: 37 thirty-minute recording periods, 1334 SWRs, N=4 mice; *CLN3⁻ᐟ⁻* n=84 thirty-minute recording periods, 2040 SWRs, N=4 mice. Bar graphs show mean +/- SEM SWR number from all recording periods, black points show mean SWR abundance for each mouse.

Supplementary Figure 8: Unlike in control mice, hippocampal sharp wave ripples (SWR) in _CLN3-/-_ mice trigger increased power in all frequency bands that lags behind and persists longer than the peak power in the SWR band.

In the major EEG frequency bands including **(A)** delta (0.1-4 Hz), **(B)** theta (4-8 Hz), **(C)** alpha (8-13 Hz), **(D)** beta (13-25 Hz), **(E)** gamma (25-50 Hz) and **(F)** high gamma (50-100 Hz), there is increased power after a SWR in _CLN3-/-_ (red) hippocampus as compared to WT (black). **(G)** While, in the SWR frequency range (150-250 Hz) there is no difference in power at the SWR peak. Group sizes for panels: WT n=2059 SWRs, N=7 mice; _CLN3-/-_ n=1363 SWRs, N=7 mice. Graphs show mean +/- SEM. Groups compared using repeated measures two-way ANOVA followed Sidak's multiple comparison test. *p<0.05, **p<0.01, ***p<0.001, ****p<0.0001.

Supplementary Figure 9: In late-stage disease, there is no difference between WT and *CLN3-/-* hippocampal sharp wave ripple (SWR) duration.
The duration of SWRs was calculated for all hippocampal ripples detected in WT (black) and *CLN3-/-* (red) 11-month-old mice. There was no significant difference in the **(A)** mean (*p*=0.43, Mann-Whitney test) or **(B)** cumulative fraction duration between groups. Bar graphs show mean +/- SEM duration of all SWRs, black points show mean SWR duration for each mouse.